Clim Dyn
DOI 10.1007/s00382-014-2104-x

# Six centuries of May–July precipitation in Cyprus from tree rings

**Ramzi Touchan · Andreas K. Christou · David M. Meko**

Received: 11 October 2013 / Accepted: 28 February 2014


**Abstract** A May–July precipitation nested reconstruction for the period AD 1415–2010 was developed from multi-century tree-ring records of *Pinus nigra*, *Pinus brutia*, and *Cedrus brevifolia* for Cyprus. Calibration and verification statistics for the period 1917–2010 show a good level of skill, and split-sample validation over 1917–2010 supports temporal stability of the tree-ring signal for precipitation. Smoothed annual time series of reconstructed precipitation and a tally of drought events in a moving time window indicate that the calibration period is not representative of the full range of drought variability. While convective precipitation in the warm season may be driven strongly by local factors, composite maps of geopotential height anomaly for dry years and wet years support large-scale atmospheric-flow influence related to height anomalies over the broader region of northeast Africa and the eastern Mediterranean. Emerging positive trend in reconstruction residuals may be an early sign of exacerbation of drought stress on trees by recent warming in May–July. Future warming expected from increases in greenhouse gases poses a threat to forest resources in Cyprus and elsewhere in the Mediterranean.

**Keywords** Tree rings · Mediterranean region · Nested reconstruction · Drought · Geopotential height

## 1 Introduction

Land degradation and depletion of water resources have exacerbated water shortages and constrained economic development in Cyprus and elsewhere in the eastern Mediterranean. The Intergovernmental Panel on Climate Change (IPCC) projects that the Mediterranean region, like other parts of the world, will likely experience a decrease in water resources due to climate change (IPCC, page 49: http://www.ipcc.ch/pdf/assessment-report/ar4/syr/ar4_syr.pdf; Kundzewicz et al. 2007), and the Mediterranean has been identified as one of the global "hotspots of climate change" Giorgi (2006). Cyprus has already experienced a decrease in precipitation in the last few decades similar to the decline in many Sahel countries (Kevane and Gray 2008). This decrease in precipitation has resulted in an even greater decrease in the country's water resources. Cyprus's dams are a buffer against drought, but have not always lived up to expectations because the majority of the dams and irrigation projects were designed on precipitation data from a wetter past.

To understand modern droughts and place them in a context of historical conditions and expected patterns of future mid-latitude drying, it is necessary to characterize the range of potential natural climate variability over the past few centuries. A few continuous high-quality instrumental climatic records in Cyprus start as early as 1916, and a record for Nicosia starts in 1878, but most records cover only the latter half of the twentieth century. Mountainous regions which encompass the forest resources and where much of the river runoff originates are especially

**Electronic supplementary material** The online version of this article (doi:10.1007/s00382-014-2104-x) contains supplementary material, which is available to authorized users.

R. Touchan (✉) · D. M. Meko
Laboratory of Tree-Ring Research, The University of Arizona, 1215 E. Lowell St. Bldg. No. 45B, Tucson, AZ 85721, USA
e-mail: rtouchan@ltrr.arizona.edu

A. K. Christou
Department of Forests, 1414 Nicosia, Cyprus

Published online: 13 March 2014

**Table 1** Site information for Cyprus

| Site name | Site code | Species | Lat. | Long. | Elev. (m) | Time span | Total no. of years | No. of trees/cores |
|---|---|---|---|---|---|---|---|---|
| Stavrostis Psokas | STP | PIBR[a] | N35.02° | E32.63° | 1,059 | 1739–2002 | 263 | 20/38 |
| Amforitis | AMF | PIBR | N35.00° | E32.63° | 859 | 1714–2010 | 297 | 21/42 |
| Tripylos | TRI | CDBR[b] | N34.99° | E32.68° | 1,352 | 1532–2010 | 479 | 42/78 |
| Amiandos | AMIB | PIBR | N34.94° | E32.92° | 1,489 | 1552–2010 | 459 | 37/77 |
| Amiandos | AMIN | PINI[c] | N34.94° | E32.90° | 1,640 | 1554–2002 | 449 | 19/33 |
| Chionistra | CHI | PINI | N34.94° | E32.87° | 1,776 | 1379–2002 | 624 | 22/44 |
| Turpland | TUL | PINI | N34.93° | E32.90° | 1,642 | 1435–2010 | 576 | 20/40 |
| Artemio | ART | PINI | N34.93° | E32.87° | 1,815 | 1410–2010 | 601 | 20/40 |
| Hatzipaylou Mine | HAM | PINI | N34.92° | E32.86° | 1,756 | 1288–2010 | 723 | 20/40 |

[a] *Pinus brutia*

[b] *Cedrus brevifolia*

[c] *Pinus nigra*

devoid of long-term climate time series. Tree-ring records allow for multi-century extension of the instrumental climate record through the development of quantitative, validated paleoclimatic reconstructions. Such reconstructions offer information on climate variability on time scales well beyond that of the instrumental data.

This paper describes the development of tree-ring chronologies of *Pinus brutia* (PIBR), *Pinus nigra* (PINI) and *Cedrus brevifolia* (CDBR) from Cyprus, and the application of the chronologies to reconstruct a 596-year time series of May–July (MJJ) precipitation. The reconstruction is analyzed to test the hypothesis that the drought history as given by the short instrumental record for Cyprus adequately represents the conditions of the past few centuries. Links between unusually dry years or wet years and large-scale atmospheric circulation are investigated with the aid of geopotential height data and teleconnection indices of modes of Northern Hemisphere upper air circulation.

## 2 Data and methods

### 2.1 Site description

The ecosystem of the Cyprus Mediterranean forests encompasses the high and steep Troodos Massif (Chionistra 1,951 m), and hills and low plains of the island. The Troodos mountain range, covering an area of about 3,200 km$^2$ and with a highest elevation of 1,951 m in Cyprus, is the main orographic feature of the island. The sampled tree-ring sites are located over an elevation range 859–1,815 m in the Troodos range (Table 1; Fig. 1). The climate is characterized by a sharp altitudinal gradient from the warm and semiarid low plains of the central part of the island (average annual temperature of about 17–19 °C; total annual rainfall of less than 300 mm) to the cold and humid higher elevations (average annual temperature of about 9–13 °C; total annual rainfall up to 1,100 mm).

### 2.2 Tree-ring data

Nine tree-ring chronologies were developed from field collections in 2002 and 2010. Samples were collected from three dominant tree species known to share a high degree of common variation strongly driven by climate (Table 1) (Touchan et al. 2014). Increment cores were taken at all sites and full cross sections were taken from stumps of cedar at a selected site. Samples were fine-sanded and crossdated and ring widths were measured to the nearest 0.01 mm using standard dendrochronological techniques (Stokes and Smiley 1968).

Each series of measured ring width was fit with a cubic smoothing spline with a frequency response of 0.50 at 67 % of the series length to remove trend possibly due to age, size, and the effects of stand dynamics (Cook and Kairiukstis 1990). The detrended series were then prewhitened with low-order autoregressive models to remove persistence, which was observed to be appreciably higher in the tree-ring series than in seasonal and annual precipitation. The resulting series is called a "residual" index. The individual indices were combined into single averaged chronologies for each combination of site and species using a bi-weight robust estimate of the mean (Cook 1985). The expressed population statistic, or EPS (Wigley et al. 1984; Cook and Kairiukstis 1990) was used to identify the period over which chronologies are well-enough replicated to capture the unknown common population tree-ring signal at a site.

### 2.3 Climate data

Station monthly precipitation and maximum and minimum temperature were obtained from the Meteorological Service of the Republic of Cyprus for a total of nine stations distributed over an elevation range 225–1,725 m (Fig. 1). The start year of monthly data for individual stations ranges from 1916 to 1978 for precipitation and 1959–1978 for

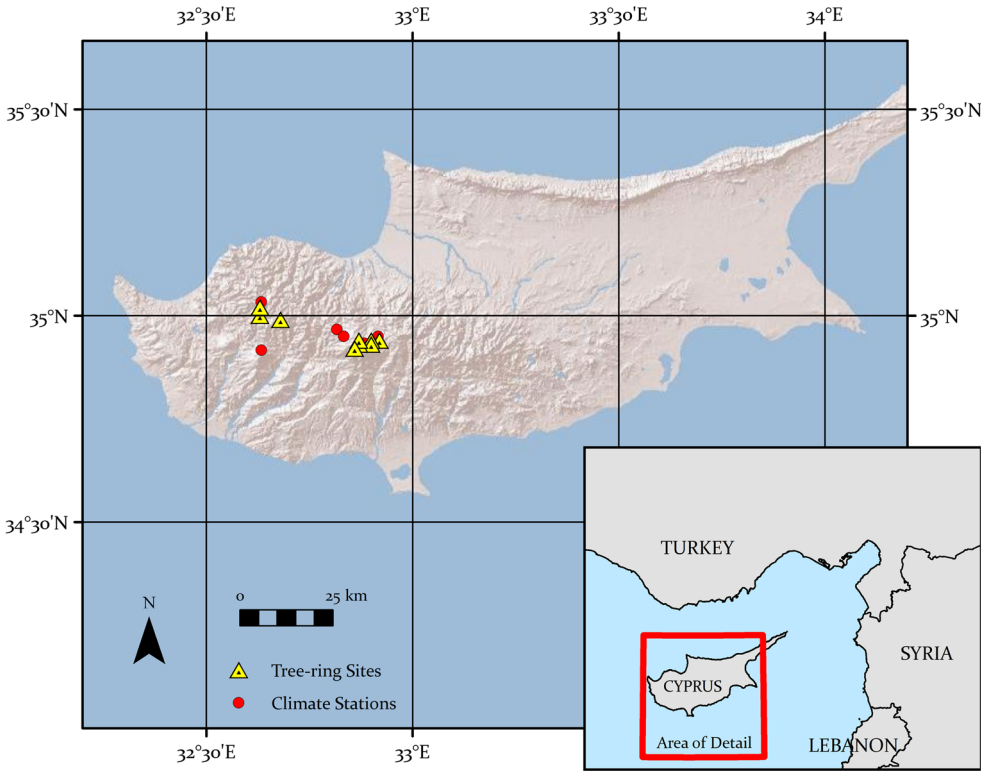


**Fig. 1** Locations of tree-ring sites and climate stations

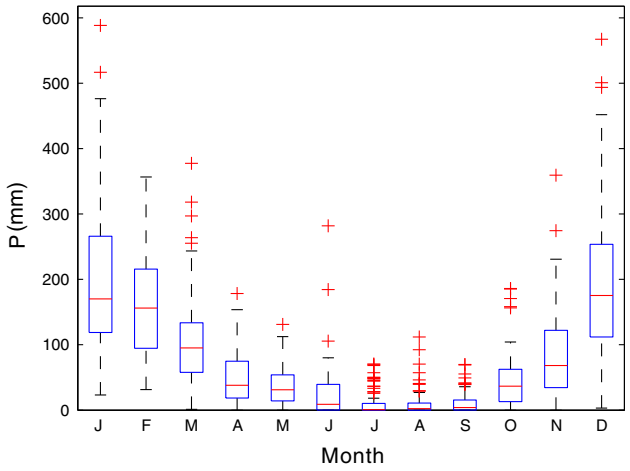


**Fig. 2** Climogram of monthly mean precipitation in Cyprus, 1917–2010. Precipitation series developed by standardized anomaly method from stations at elevation 1,080 m and higher in Cyprus (see text). Mean annual total 934 mm, of which 73 mm, or 7.8 %, falls in MJJ

temperature Exploratory correlation analysis indicated that correlations of tree-ring chronologies with seasonal-total precipitation is higher for high-elevation stations than for low-elevation stations, which is consistent with the higher-elevation locations of the tree-ring sites. Accordingly, a regional monthly precipitation series, 1916–2012, based on just the four stations at elevation 1,080 m or higher was computed by the method of averaged standardized anomalies (Jones and Hulme 1996) for use in calibration tree-ring reconstruction models. The regional precipitation series is computed from complete monthly data at all four stations for years 1961–2011; earlier parts of the series are based on fewer stations, but two stations have complete monthly data back to 1917. A regional time series of monthly average daily maximum temperature, 1959–2012, was similarly computed from five stations with temperature data. A climogram of monthly precipitation from the regional series emphasizes the Mediterranean precipitation regime of Cyprus (Fig. 2). Monthly precipitation drops sharply from the wetter winter months through late spring, and typically reaches lows in July and August.

A longer time series, 1878–2000, of monthly precipitation for Nicosia, at sea level in Cyprus was obtained from the Cyprus Meteorological Service for use in corroborating reconstructed precipitation variations prior to the period of calibration/validation of the precipitation reconstruction models. Gridded precipitation from the Cru T3 dataset over Cyprus (34.5°–35°N, 32.50°–33°E) were downloaded from KNMI Climate Explorer web site (http://climexp.knmi.nl/start.cgi?someone@somewhere) and explored to gauge the relative merits of gridded-network and station climate data for summarizing the strength of climatic signal in the Cyprus tree-ring widths.

Association of extremely dry or wet years in Cyprus with atmospheric circulation anomalies was studied with the aid of composite maps of 500 mb geopotential height

anomaly drawn with the mapping tool of the NOAA/ESRL Physical Sciences Division (http://www.esrl.noaa.gov/psd/) snd NCEP/NCAR Reanalysis data (Kalnay et al. 1996). Recent trends in primary modes of low-frequency upper air circulation active in the warm season were summarized with linear regression against time of indices of Northern Hemisphere teleconnection patterns downloaded from the National Weather Service Climate Prediction Center (CPC) (http://www.cpc.ncep.noaa.gov/).

### 2.4 Reconstruction

The season for precipitation reconstruction was selected with the aid of program Seascorr, which computes correlations and partial correlations between tree-ring data and monthly precipitation and temperature data integrated over seasons of variable length (Meko et al. 2011).

The reconstruction model was derived by ordinary least squares (OLSs) regression (Weisberg 1985) of seasonal total precipitation on principal components of the individual residual site chronologies. Predictors for the final nested reconstruction models were selected from the full pool of available PCs by stepwise regression with $p$-to-enter and $p$-to-remove set at 0.15, and the adjusted $R^2$ and Mallows's $C_p$ statistic (Mallows 1973) were used as guides to guard against overfitting. A nested reconstruction was developed to accommodate the varying chronology lengths while exploiting the potential to accurately capture the long-term history of extreme events (Touchan et al. 2008). In the nested approach, the full tree-ring record is divided into a small number of overlapping sub-periods, each fully covered by some distinct set of chronologies. A separate reconstruction model is developed for each sub-period. The reconstructions by these nested models are ultimately blended into a single final reconstruction. When reconstructed values are available from multiple models for some year or segment of the long-term record, the value from the "best" model is preferred. We define "best" for this study as the model with the largest number of chronologies. The nested procedure allows for a maximum length reconstruction, although the earliest part of a record may be reduced in robustness because of thin sample size—fewer chronologies for earlier nested models, and gradually diminishing number of trees toward the start of those chronologies. The period of detailed analysis of the reconstruction was truncated in accordance with EPS evidence of the reliable portions of component tree-ring chronologies. The strength of the reconstruction models was examined using regression and correlation statistics. Models were cross-validated by the predicted error sum-of-squares (PRESS) method (Weisberg 1985; Fritts et al. 1990; Meko 1997; Touchan et al. 1999, 2003, 2005a, b). The PRESS method is equivalent to leave-one-out cross-validation, in which a model is validated iteratively by repeated calibration and validation, each time leaving one observation out of the calibration set and applying the model to predict the omitted observation. Model stability was checked by split-sample validation (Snee 1997; Meko and Graybill 1995; Touchan et al. 2003, 2005a, b), in which the full available calibration period was divided in half. Skill of reconstruction compared with that of a simple model with the calibration-period mean of observed precipitation as the reconstruction was checked with the reduction of error statistic (Fritts et al. 1990). Low-frequency time series variations in reconstructed precipitation were summarized with 10-year moving averages of the annual reconstruction. Changes in drought frequency through time were summarized by a count of number of years below a specified drought threshold in a 50-year moving window.

## 3 Results and discussion

### 3.1 Chronology development

The lengths of the nine chronologies range from 263 to 723 years (Table 1). Statistics for each chronology are listed in Table 2. The mean correlation among individual radii at each site represents the strength of their common signal and ranges from 0.30 to 0.46. As expected, chronologies with a stronger common signal also tend to have a greater variability, as measured by the chronology standard deviation, and a higher percentage of variance explained by the first principal component of core indices. The chronologies are generally heavy-tailed relative to a normal distribution, as reflected by the kurtosis (Table 2). This trait and predominantly positive skew lead to rejection of a null hypothesis of normality at the 0.01 $\alpha$-level for six of the nine chronologies in an Anderson–Darling test (1954), which tests statistically whether a sample of data is drawn from a specified probability distribution. Positive skew in chronologies was not regarded as a problem for our study, as monthly precipitation and seasonal-total precipitation in Cyprus are also positively skewed.

The mean sample segment length (MSSL) of the nine chronologies ranges from 169 to 332 years. Eight of these chronologies have MSSL greater than 200 years in length. Therefore, with monotonic or conservative detrending choices, the chronologies should be suitable for investigating low-frequency climate variability on decadal to century time scales. The EPS statistic indicates that by the late 1700s individual chronologies are sufficiently well replicated to capture the population growth-signal at each site.

**Table 2** Summary statistics for the nine chronologies for the ARSTAN program

| Site code | MSSL | Total chronology | | | | No. of trees | Common interval | | |
|---|---|---|---|---|---|---|---|---|---|
| | | Std | SK | KU | 1st year EPS > 0.85 | | Time span | MCAR | EV PC1 (%) |
| STP | 213 | 0.16 | −0.02 | 1.15 | 1773 | 10 | 1829–2002 | 0.37 | 39 |
| AMF | 169 | 0.17 | −0.03 | 0.64 | 1779 | 10 | 1844–2010 | 0.37 | 40 |
| TRI | 241 | 0.19 | 0.54 | 2.80* | 1718 | 10 | 1813–2002 | 0.37 | 38 |
| AMIB | 202 | 0.17 | 0.34 | 1.08 | 1734 | 09 | 1842–2002 | 0.40 | 42 |
| AMIN | 325 | 0.14 | 0.16 | 0.61* | 1591 | 14 | 1640–1934 | 0.30 | 33 |
| CHI | 332 | 0.19 | 0.62 | 0.81* | 1635 | 09 | 1727–2002 | 0.41 | 44 |
| TUL | 315 | 0.18 | 0.50 | 2.64* | 1605 | 09 | 1788–2010 | 0.41 | 43 |
| ART | 332 | 0.18 | 0.41 | 0.16* | 1632 | 10 | 1731–1998 | 0.37 | 40 |
| HAM | 275 | 0.21 | 0.07 | 5.26* | 1629 | 07 | 1786–2006 | 0.46 | 48 |

*MSSL* mean sample segment length, *Std* is standard deviation, *SK* skewness, *KU* Kurtosis, *EPS* Expressed Population Statistic (Wigely et al. 1984), *MCAR* mean correlation among radii, *EV* is explained variance by 1st PC

* Fails Anderson–Darling normality test at $\alpha = 0.01$ (Anderson and Darling 1954)

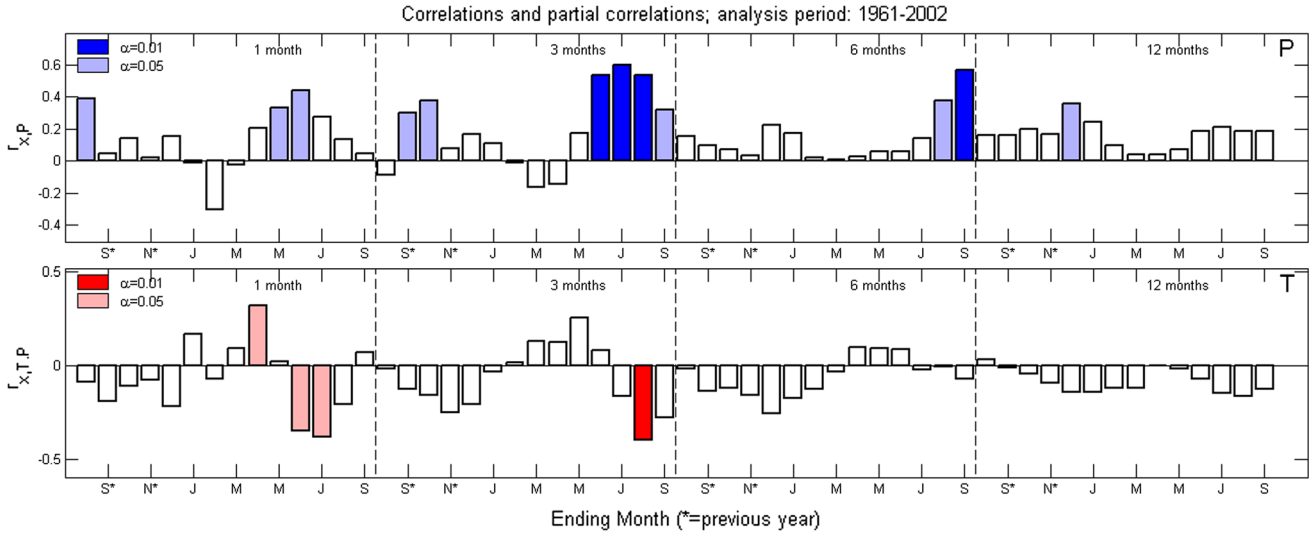


**Fig. 3** Program Seascorr summary of seasonal climatic signal in tree-ring data. The tree-ring variable is the score time series of the first principal component (PC1) of nine residual tree-ring chronologies (PC analysis described in text). Climatic variables are regional-average monthly precipitation and temperature (daily maximum) as defined in the text. (*Top*) Correlation of tree-ring variable with monthly, 3-month total, 4-month total and 6-month total precipitation for ending months from August preceding the growth year through September of the growth year. (*Bottom*) Partial correlations (controlling for precipitation) of tree-ring variable with monthly average temperature. *Colors* indicate Monte-Carlo-derived significance of correlation or partial correlation (Meko et al. 2011) for α-levels 0.01 and 0.05. Analysis period is tree-ring years 1961–2002

### 3.2 Climate signal and reconstruction

MJJ total precipitation total was selected as a reconstruction target (predictand for reconstruction model) based on program Seascorr (see Sect. 2) results relating the first principal component of the nine residual chronologies, 1917–2002, to regional precipitation and maximum temperature (Fig. 3). That analysis identifies May precipitation as the single month of greatest precipitation influence and May–July as the most important 3-month period (Fig. 3). Exploration of various window lengths, or aggregation periods, with Seascorr indicated declining correlation for seasons longer than 3 months duration. Temperature influence, summarized by partial correlations in Seascorr, is significant for the single months of June and July. The negative sign of partial correlations for those months indicates that high temperature exacerbates the negative tree-growth anomaly associated with a given precipitation deficit.

May to July total precipitation for the four-station regional series, heretofore referred to as "precipitation", was applied as the predictand in three different nested reconstruction models with varying time coverage and chronology makeup (Tables 3, 4). Stepwise regression with adjusted $R^2$ and Mallow's $C_p$ as guides resulted in just one or two PCs as predictors for the different models, and in all cases PC1 was the first predictor to enter. Nested models calibrated on 1917–2002 or 1917–2010 explain 38–45 %

**Table 3** Summary statistics of nested reconstruction models

| Reconstructions model[a] | Variable | Coefficient | Adjusted-$R^2$ calibration | PRESS | No. of chronologies |
|---|---|---|---|---|---|
| M1741 | Constant | 72.9 | 0.45 | 0.39 | 9 |
| | PC1 (56 %)[b] | 14.0 | | | |
| | PC3 (9 %) | −19.0 | | | |
| M1718 | Constant | 74.2 | 0.41 | 0.36 | 6 |
| | PC1 (55 %) | 16.9 | | | |
| | PC3 (12 %) | 16.8 | | | |
| M1415 | Constant | 71.0 | 0.38 | 0.33 | 3 |
| | PC1 (80 %) | 20.6 | | | |

[a] Model coded by start year of segment of reconstruction period. All models

[b] Proportion of tree-ring variance accounted for

**Table 4** Split-sample calibration and validation statistics of three reconstruction models

| Reconstruction model[a] | Calibration period | Verification period | Adjusted-$R^2$ calibration | $r^2$-verification | Reduction of error (RE) |
|---|---|---|---|---|---|
| M1741 | 1917–1959 | 1960–2002 | 0.50 | 0.42 | 0.27 |
| M1718 | 1917–1963 | 1964–2010 | 0.47 | 0.39 | 0.19 |
| M1415 | 1917–1959 | 1960–2002 | 0.44 | 0.34 | 0.22 |
| M1741 | 1960–2002 | 1917–2002 | 0.39 | 0.53 | 0.46 |
| M1718 | 1964–2010 | 1917–1963 | 0.37 | 0.48 | 0.40 |
| M1415 | 1960–2002 | 1917–1959 | 0.32 | 0.45 | 0.40 |

[a] Model coded by start year of segment of reconstruction period. All models

of the calibration-period variance, according to the regression adjusted $R^2$. Time plots of reconstructed and observed precipitation for the calibration periods of the three models are included in the Fig. 1 in the Supplemental Materials. The start years of the nested reconstructions are 1415, 1718, and 1741; the number of chronologies contributing to those models is 3, 6 and 9, respectively. For brevity, we refer to the models by start year: M1415, M1718 and M1741.

The residuals for all three models listed in Table 3 pass an analysis-of-residuals check for possible violation of regression assumptions. None of the residual series have significant autocorrelation or linear trend ($t$ test of slope of best-fit straight line). For none of the residual series can the assumption of normality be rejected at $\alpha = 0.01$ by the Anderson–Darling test, and no systematic pattern is obvious in scatterplots of residuals on fitted values.

The small drop from adjusted $R^2$ to prediction $R^2$ (PRESS statistic) for the models (Table 3) suggests that the models have not been over fit. All models have positive RE statistic for cross-validation. Stability of the models is also supported by results of the split-sample calibration–validation (Table 4).

The $R^2$ values for these models, while modest compared to values found in some dendroclimatic reconstructions (e.g., Meko et al. 2011; Touchan et al. 2008; Woodhouse et al. 2006), are high considering that MJJ precipitation comprises less than 8 % of the annual total precipitation in Cyprus. Perhaps such a response is expected because precipitation is more likely to limit growth in this normally dry season. Winter snowpack largely gone and winter moisture evaporated from the root zone by the time cambial growth begins, such that whatever rain does occur in MJJ is critical to growth. Tree-ring studies in Turkey (e.g., Touchan et al. 2003, 2005a, b, 2007; Köse et al. 2011; Akkemik et al. 2008) have previously identified late spring and early summer as key months in the eastern Mediterranean for precipitation influence on tree growth.

It is important to recognize that the assessed strength of precipitation signal in the Cyprus tree-ring chronologies is dependent on reliable observed precipitation from mountain stations, as in our regional series used to calibrate the reconstruction models. Exploratory analysis showed that while the regional precipitation series based on station data from four higher-elevation Cyprus stations yields $R^2 = 0.45$ for reconstruction of MJJ precipitation, gridded precipitation from CRU TS 2.1 (Mitchell and Jones 2005) and the identical calibration period and predictors has $R^2 = 0.06$. This shortcoming of the gridded data probably stems from limitation of the interpolation process in capturing precipitation variations that may be of practical importance to a small region, such as the Island of Cyprus. The stations contributing to individual grid-point precipitation are unknown to the user of the gridded data, but possibly stations from sea level or remote locations contributed substantially to the points near Cyprus.

We also note that use of a recent segment of the full available 1917–2010 period of overlap of tree rings and

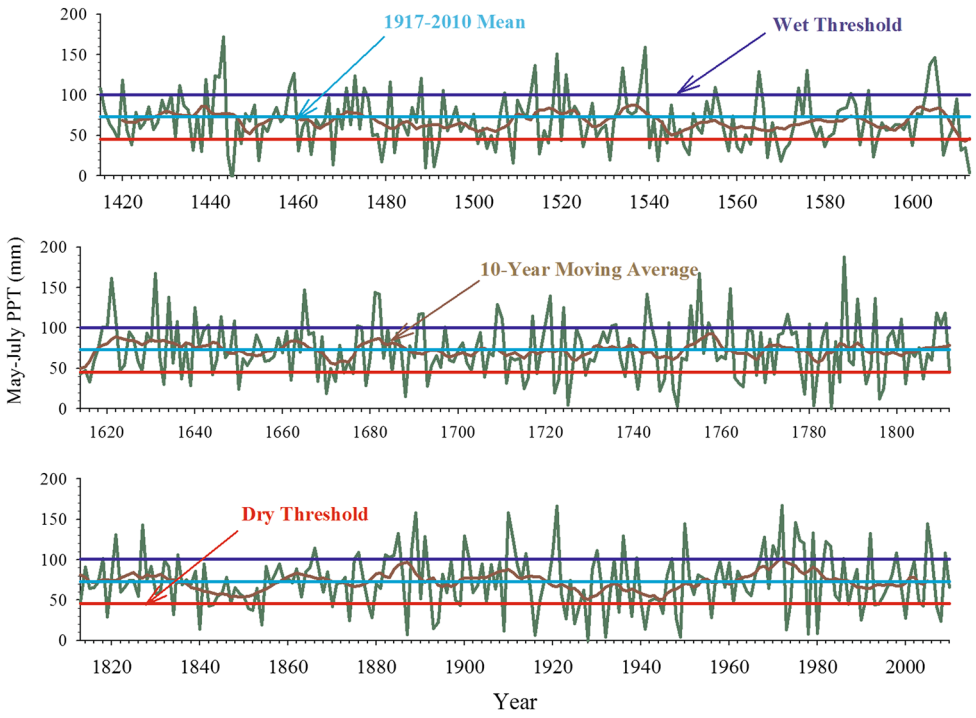


**Fig. 4** Time series plot of reconstructed May–July precipitation, AD 1415–2010

precipitation data for model calibration can yield higher estimates of reconstruction accuracy than we report for our reconstructions (see Table 3). Using 1970–2010, for example as a calibration period would give adjusted $R^2 = 0.55$ for model M1741.

The long-term reconstructed time series of MJJ precipitation covers the period 1415–2010 (Fig. 4). The uncertainty, or error, in reconstruction varies by nested model, such that the part starting in 1741 is most robust. This model includes nine tree-ring chronologies, seven of which have already reached a critical EPS of 0.85 by 1741. This model also has the highest accuracy of the three models according to calibration statistics. The broadened time-window of the reconstruction models gives information on possible short-term bias of precipitation statistics for the instrumental period. The bias can be assessed by comparison of statistics of the long-term and calibration-period reconstruction for a particular nested model. For model M1741, the empirical cumulative distribution functions (CDFs) for 1917–2002 and 1741–2002 are similar, except for the longer tail for 1741–2002 driven by the single high value (187 mm) prior to the calibration period (Fig. 5). Otherwise, the short-term bias is small: the CDFs for percentiles below the 100th percentile differ at most by just 9 mm (Fig. 5, dashed line).

For a tally of droughts and wet periods, dry and wet years in the MJJ precipitation plotted in Fig. 5 are arbitrarily delineated by reconstructed precipitation below the 25th or above the 75th percentile (45.42 and 100.45 mm respectively) computed for 1917–2002. Our quantitative

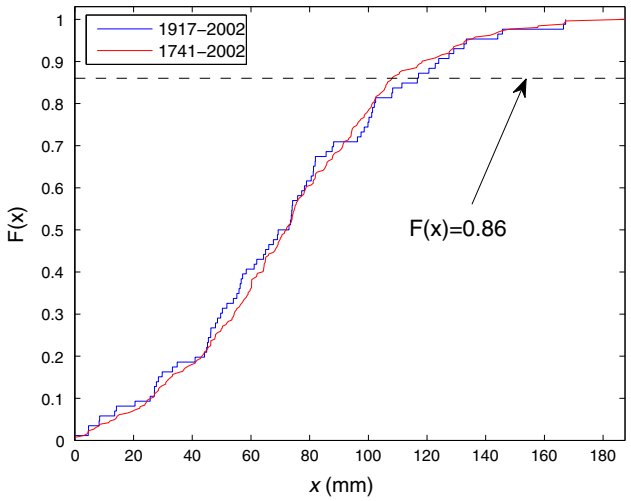


**Fig. 5** Short-term bias of CDF of reconstructed precipitation. CDFs are shown for the calibration period and full reconstruction period of M1741, the best-replicated reconstruction model. Plotted variable, $F(x)$, is the empirical probability that precipitation is less than or equal to $x$. Annotated is the 86th percentile, where the two plotted CDFs differ most, and where the short-term record is biased wet by 9 mm (117 vs 108 mm) relative to the long-term record

drought assessment is restricted to the part of the reconstruction starting with 1741 to avoid including droughts indicated by the less robust M1415. However, the M1415 model does become robust after about 1635, when the three long chronologies reached a critical EPS of 0.85. For the period 1741–2010, the reconstruction has 60 dry years, defined as precipitation below the dry threshold. Thirty-

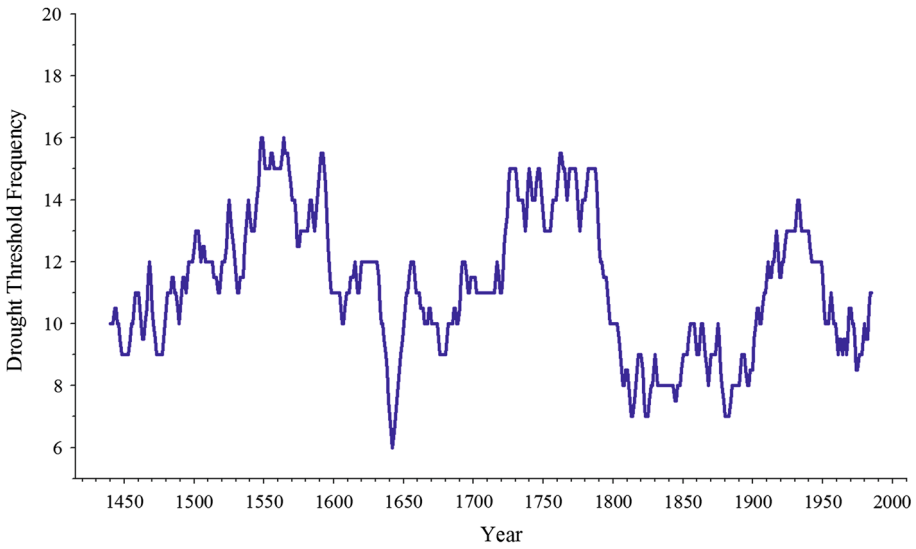


**Fig. 6** Time plot of sum of dry years in a moving 50-year window. Sum plotted at center of 50-year period

nine drought events have duration 1 year, seven have duration 2 years, and three have duration 3 years (1763–1765). The driest single year of the reconstruction is 1928 (0.0 mm; instrumental is 4.9 mm). The driest year in the instrumental data is 1949 (0.0 mm; reconstructed is 4.6 mm).

Several historical events of drought for Anatolia and neighboring countries coincide with extreme dry years in May–July precipitation reconstructions, such as 1725 (Touchan et al. 2003, 2005a, b, 2007; Akkemik et al. 2005; Ottoman Archives 1850–1930; Inalcik 1997; Purgstall 1983), 1887 (D'Arrigo and Cullen 2001; Touchan et al. 2003, 2005a, b, 2007; Akkemik et al. 2005; Inalcik 1997), and 1910 (D'Arrigo and Cullen 2001; Hughes et al. 2001; Akkemik et al. 2005).

The long term reconstruction contains 59 wet years, or years wetter than the specified wet threshold. Thirty-two wet events have duration 1 year, ten events have duration 2 years, three events have duration 3 years, and one event has duration 4 years (1882–1885). The wettest single year of the reconstruction is 1788 (187 mm), while the wettest single year in the instrumental data is 1921 (369 mm).

A 10 year moving average of the reconstruction demonstrates multi-annual to decadal variation in MJJ precipitation and suggests several prolonged wet and dry events (Fig. 4). The driest 10-year reconstructed period is 1940–1949 (51 mm). The driest 10-year in the reconstruction from 1415–2010 is 1607–1616. The wettest 10-year reconstructed period is 1967–1976 (102 mm) and was a period of exceptionally high growth. Some persistent multi-decadal intervals of gradually declining precipitation are evident in the time plot of 10-year running means (Fig. 4). The most prominent 10 year trend is 1842–1854. In contrast, some extended periods (e.g., 1792–1820) are characterized by low variability at decadal and longer scales.

A 50 year moving average of the reconstructed drought frequency during the robust period 1741–2010 demonstrates that frequency of dry years is highest for 1744–1793 and lowest for 1799–1907 (Fig. 6). However, the highest drought frequency in the nested reconstruction from 1415–2010 is from 1524–1588 and the lowest is from 1615 to 1668.

Our precipitation reconstruction is significantly correlated ($r = 0.70$, $n = 260$, $p \leq 0.0001$) with May–August precipitation, 1400–2000, reconstructed by Touchan et al. (2005b) for the eastern Mediterranean. Our reconstruction includes four chronologies that were used in Touchan et al. (2005b) (AMIN, AMIB, STP, and CHI). The 1887–2000 segment of the reconstruction is also significantly correlated ($r = 0.36$, $n = 114$, $p = 0.0001$) with MJJ total precipitation measured at the sea level station Nicosia, Cyprus. Our reconstruction is also significantly correlated ($r = 44$, $n = 30$, $p < 0.013$) with the part of the Nicosia precipitation record (1887–1916) that predates the start of our calibration/validation period.

### 3.3 Climatology

The May–July precipitation reconstructed here falls outside the main precipitation season (cool season) in Cyprus. In fact, MJJ accounts for less than 8 % of the annual total precipitation, 1917–2010, in the regional series (see Fig. 2). Accordingly, attention has been directed toward understanding the climatology of cool-season rather than warm-season precipitation in this region (e.g., Xoplaki et al. 2004). Likewise, historical precipitation studies have centered mainly on the western Mediterranean and cool season (Camuffo et al. 2010, 2013; Luterbacher et al.

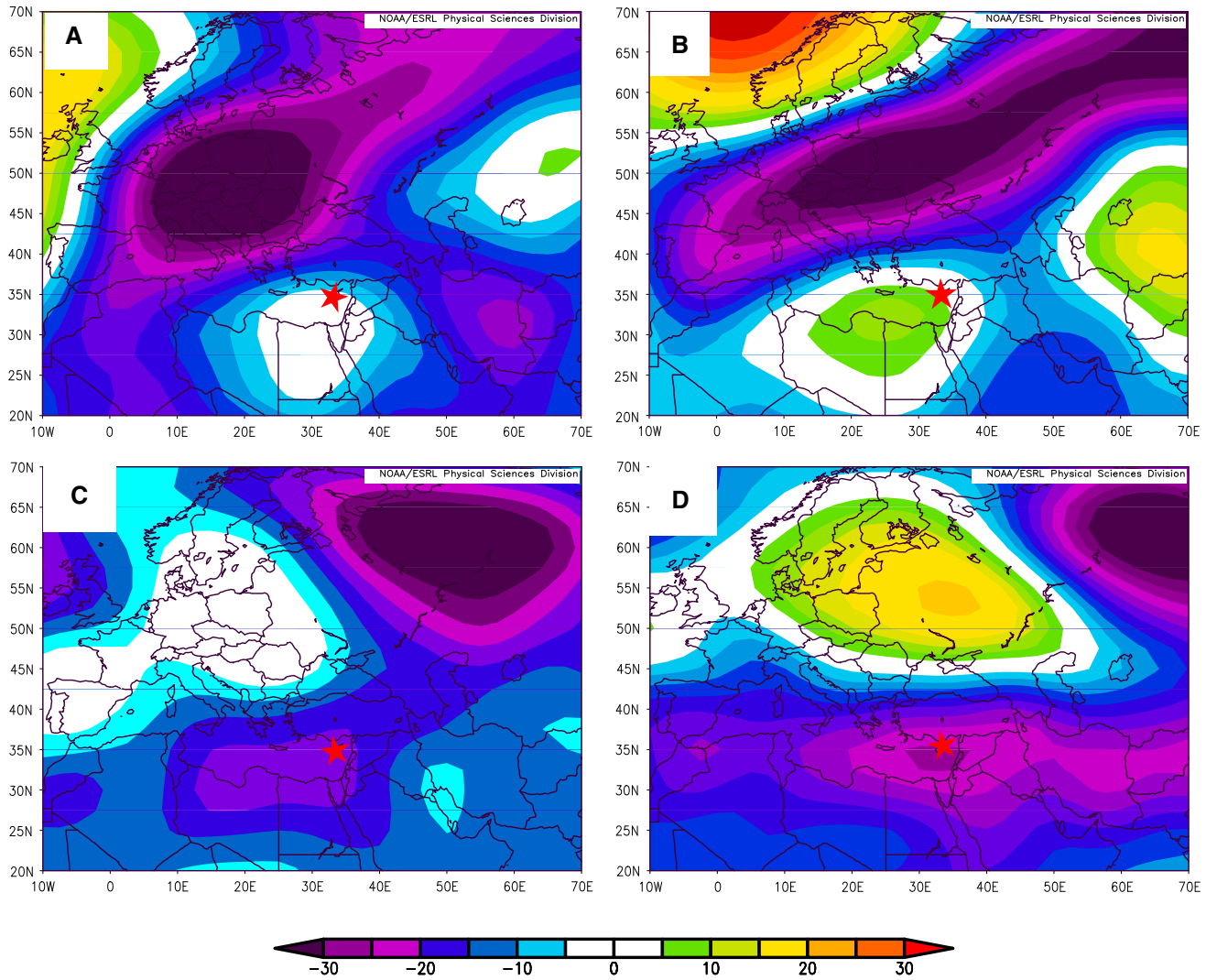


**Fig. 7** Composite May–July 500 mb geopotential height anomaly maps for driest and wettest 6 years in Cyprus, 1949–2010. **a** Driest observed, **b** driest reconstructed, **c** wettest observed, **d** wettest reconstructed. *Red star marks* Cyprus. Units of anomalies are tens of meters. Years for composites are as follows: [**a** 1949, 1978, 1966, 1990, 1991, 1955], [**b** 1949, 1978, 1980, 1973, 2008, 1990], [**c** 2007, 1982, 1979, 1963, 1999, 1976], [**d** 1992, 1979, 1950, 2005, 1975, 1972]. Maps of 500 mb gph anomaly for the individual years of the four composites are included as Figs. 2, 3, 4, and 5 in the Supplemental Materials

2010). Small-scale factors are likely to be more influential in the warm season, which is characterized by convective precipitation than in the cool season, which is characterized organized precipitation systems associated with cyclones in the westerlies. The association of wettest and driest years with circulation anomalies was studied with maps of average 500 mb geopotential height anomaly for driest and wettest Cyprus years, 1949–2010 (Fig. 7). Composites were built on roughly the driest and wettest decile, or 6 years, of the analysis period. Although the years for a particular (wet or dry) composite are not exactly the same for the observed and reconstructed precipitation, the reconstructed composites are robust in that no year listed in the dry (wet) reconstructed composite has observed precipitation above (below) the median observed precipitation for 1949–2010.

The composite maps suggest some link of MJJ precipitation anomalies with large-scale atmospheric circulation. For the dry-composite 500 mb patterns for both the observed and reconstructed precipitation, Cyprus lies at the northeastern edge of an anomalous high over the eastern Mediterranean or eastern North Africa, with anomalously strong westerly flow over the Balkans or southern Europe (Fig. 7a, b). This flow pattern would hinder development of late spring cyclones in the region and favor stability and suppression of summer convective storms. The wet composites for observed and reconstructed precipitation are less similar overall, but share the consistent feature of

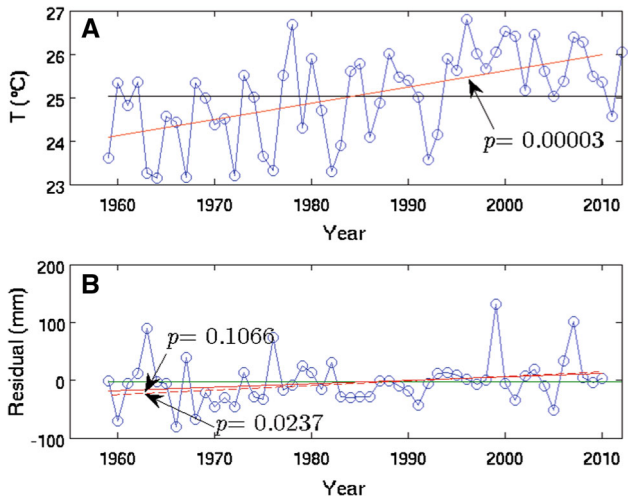


**Fig. 8** Parallel trends in maximum daily temperature and reconstruction residuals, 1970–2010. **a** Maximum daily temperature, *T*. **b** Reconstruction residuals, $e_t$. The temperature series is a 5-station regional May–July (MJJ) average for Cyprus, as described in text. The reconstruction residuals are observed minus MJJ precipitation reconstructed by model M1741 for years 1970–2002 and by model M1718 for years 2003–2010. Annotated on the plots are least-squares fits of the variable against time (year), with the *p* value of the *t*-statistic for the estimated slope. In **b**, *solid line* is slope estimated with all years, 1970–2010, and *dashed line* is slope estimated with 1976 and 1999 omitted from sample

anomalous low pressure over North Africa or the Mediterranean Sea, and anomalous flow from the south or southeast over Cyprus (Fig. (7c, d). The anomaly patterns of 500 mb height therefore appear to be consistent with the dry-year and wet-year composites, although considerable variability in MJJ mean flow patterns and anomalies can be seen in plots for individual years of the composites (Auxilliary Material).

Considering the vulnerability of the Mediterranean region to warming and desertification in response to future climate change, recent climatic trends are of particular interest (e.g., IPCC Report 2007). Linear regression of MJJ monthly average daily maximum temperature (regional-average series describe previously) on time, 1959–2010, shows a significant ($\alpha = 0.01$) positive trend (Fig. 8a). For a semi-arid region such as Cyprus, increasing temperature would logically exacerbate physiological drought-stress on the trees beyond the level commensurate with reduced precipitation. Indeed, Seascorr results presented earlier indicate significant negative partial correlation of tree-ring index with temperature when both variables are controlled for precipitation (see Fig. 3). While the corresponding linear trend in reconstruction residuals (observed minus reconstructed MJJ precipitation), 1917–2010 is not statistically significant at $\alpha = 0.05$, the positive slope of the trend line is consistent with warming inducing a gradual reduction in growth. This effect may be masked in the available data by the over-riding influence of high frequencies on the variance of the residuals, particularly the influence of the large residuals (e.g., 1963). Omission of just one of those outlier observation (1963) yields a statistically significant ($\alpha = 0.05$) positive trend in residuals (dashed line in Fig. 7b). If the time-trend in residuals is indeed real and related to increasing MJJ temperature, two important implications should be noted. First, tree-growth and forest production in Cyprus are likely to decline in the future even if MJJ precipitation remains at current levels. Second, a caveat must accompany climatic interpretation of past, pre-instrumental, reconstructed precipitation: reconstructed lows (highs) in precipitation may to some extent reflect periods of cooling (warming).

The temperature trend evident in Fig. 8a may be associated with trends in modes of large-scale atmospheric circulation. The North Atlantic Oscillation (NAO) and East Atlantic pattern (EA) are two prominent modes of Northern Hemisphere atmospheric circulation with a presence in the summer months and characteristic precipitation and temperature anomaly fields that might be expected to influence climate in Cyprus (see http://www.cpc.ncep.noaa.gov/data/teledoc/telecontents.shtml). For the period of positive temperature trend in MJJ Cyprus temperature (Fig. 8a), NAO averaged for MJJ was found to have a statistically significant linear negative trend ($p < 0.05$) and EA a statistically significant positive trend ($p < 0.01$). The EA trend, in particular, is strong over the full period, and is consistent with warming in Cyprus because the positive EA mode is characterized by an anomalous 500 mb high extending zonally across the Mediterranean (http://www.cpc.ncep.noaa.gov/data/teledoc/telecontents.shtml). This high is consistent with the dry-composite 500 mb patterns in Fig. 7, with subsidence, suppression of summer convection, and shunting of spring cyclones away from Cyprus. As emphasized by others (e.g., Touchan et al. 2005b), it is important to keep in mind that warm-season precipitation is typically convective, often highly localized, and dependent on conditions such as insolation, instability, local topography, and winds. As such, warm-season precipitation may be much more problematic than temperature to link to large-scale atmospheric circulation anomalies.

## 4 Conclusion

An understanding of natural climate variability over several centuries is important for natural resource managers and planners to implement low-risk, long-term plans to achieve conservation and sustainable use of water and other natural resources. This study attests to the value of tree-ring widths for long-term information on precipitation in the late spring to early summer in Cyprus. The identified

droughts of the past few centuries should help resource managers assess vulnerability of forests and other resources to warm-season precipitation fluctuations. Results presented here suggest the period covered by instrumental data falls short in identifying possible wet and dry extremes on decadal and longer time scales. Maps of 500 mb geopotential height anomaly for composites support a link of extreme years (wet or dry) with large-scale circulation anomalies extending over a broad region including North Africa, the eastern Mediterranean, and the Balkans. Future warming poses a serious threat to water resources, forest resources and agriculture in Cyprus and elsewhere, and our results suggest some incremental stress on tree-growth—beyond that due to precipitation fluctuations—from rising MJJ temperatures. One limitation of the current study is the thin sample size of tree-ring data and concomitant increased uncertainty of reconstruction prior to the mid-1700s. Future field collections of increment cores and possibly remnant wood may help mitigate this problem. Future studies should also focus on exploiting additional tree-ring species and measurement variables (e.g., earlywood/latewood width, density, stable isotopes) to not only strengthen the signal for warm-season precipitation, but to address long-term variability of cool-season precipitation, which is the primary water resource for Cyprus.

**Acknowledgments** The authors wish to thank the Cyprus Ministry of Agriculture, Department of Forestry, and the Cyprus Forestry College, Mr. Konstantinos Rovanias and Mr. Loizos Constantinou for their help and support. We thank Christopher Baisan, Elina Minaidou, Loizos Constantinou for his valuable help in the field. We thank Martin Munro for helping with the graphics. Funding was provided by the US National Science Foundation under Grant Earth System History (Grant No. 0075956) and ATM-GEO/ATM-Paleoclimate Program 0758486.

## References

Akkemik Ü, Dağdeviren N, Aras A (2005) A preliminary reconstruction (A.D. 1635–2000) of spring precipitation using oak tree rings in the western Black Sea region of Turkey. Int J Biometeorol 49:297–302

Akkemik Ü, D'Arrigo R, Cherubini P, Köse N, Jacoby GC (2008) Tree-ring reconstructions of precipitation and streamflow for north-western Turkey. Int J Climatol 28:173–183

Anderson TW, Darling DA (1954) A test of goodness-of-fit. J Am Stat Assoc 49:765–769

Camuffo D, Bertolin C, Diodato N, Barriendos M, Dominguez-Castro F, Cocheo C, della Valle A, Garnier E, Alcoforado MJ (2010) The western mediterranean climate: how will it respond to global warming. Clim Change 100:137–142

Camuffo D, Bertolin C, Diodato N, Cocheo C, Barriendos M, Dominguez-Castro F, Garnier E, Alcoforado MJ, Nunes MF (2013) Western mediterranean precipitation over the last 300 years from instrumental observations. Clim Change 117:85–101

Cook ER (1985) A time-series analysis approach to tree-ring standardization. Ph.D. Dissertation. Department of Geosciences, The University of Arizona, Tucson

Cook E, Kairiukstis L (1990) Methods of dendrochronology: applications in the environmental sciences. Kluwer Academic, Doredrecht

D'Arrigo RD, Cullen HM (2001) A 350-year (AD 1628–1980) reconstruction of Turkish precipitation. Dendrochronologia 19:169–177

Fritts HC, Guiot J, Gordon G (1990) Verification. In: Cook ER, Kairiukstis LA (eds) Methods of dendrochronology: applications in the environmental sciences. International Institute for Applied Systems Analysis Kluwer Academic, Boston, pp 178–184

Giorgi F (2006) Climate change hot-spots. Geophys Res Lett 33:L87070

Hughes MK, Kuniholm PI, Garfin GM, Latini C, Eischeid J (2001) Aegean tree-ring signature years explained. Tree-Ring Res 57(1):67–73

Inalcik H (1997) A note on the population of Cyprus. http://www.mfa.gov.tr/grupa/percept/ll2/II2-3.html

Jones PD, Hulme M (1996) Calculating regional climatic time series for temperature and precipitation: methods and illustrations. Int J Climatol 16:361–377

Kalnay E et al (1996) The NCEP/NCAR reanalysis 40-year project. Bull Am Meteorol Soc 77:437–471

Kevane M, Gray L (2008) Darfur: rainfall and conflict. Environ Res Lett 3:034006

Köse N, Akkemik Ü, Dalfes HN, Özeren MS (2011) Tree-ring reconstructions of May–June precipitation for western Anatolia. Quat Res 75:438–450. doi:10.1016/j.yqres.2010.12.005

Kundzewicz ZW, Mata LJ, Arnell NW, Doll P, Kabat P, Jimenez B, Miller KA, Oki T, Sen Z, Shiklomanov IA (2007) Freshwater resources and their management. In: Parry ML Parry, Canziani OF, Palutikof JP, van der Linden PJ, Hanson CE (eds) Climate Change 2007: impacts, adaptation and vulnerability. Contribution of Working Group II to the Fourth Assessment Report of the Intergovernmental Panel on Climate Change. Cambridge University Press, Cambridge, UK, 173–210

Luterbacher J, Koenig SJ, Franke J, van der Schrier G, Zorita E, Moberg A, Jacobeit J, Della-Marta PM, Küttel M, Xoplaki E, Wheeler D, Rutishauer T, Stössel M, Wanner H, Brázdil R, Dobrovolný P, Camuffo D, Bertolin C, van Engelen A, Gonzalez-Rouco FJ, Wilson R, Pfister C, Limanówka D, Nordli Ø, Leijonhufvud L, Söderberg J, Allan R, Barriendos M, Glaser R, Riemann D, Hao Z, Zerefos CS (2010) Circulation dynamics and its influence on european and mediterranean January–April climate over the past half millennium: results and insights from instrumental data, documentary evidence and coupled climate models. Clim Change 101:201–234

Mallows CL (1973) Some comments on Cp. Technometrics 15:661–675

Meko DM (1997) Dendroclimatic reconstruction with time varying subsets of tree ring indices. J Clim 10:687–696

Meko DM, Graybill DA (1995) Tree-ring reconstruction of Upper Gila River discharge. Water Resour Bull 31:605–616

Meko DM, Touchan R, Anchukaitis KJ (2011) Seascorr: a MATLAB program for identifying the seasonal climate signal in an annual tree-ring time series. Comput Geosci 37(9):1234–1241

Mitchell T, Jones P (2005) An improved method of constructing a database of monthly climate observations and associated high-resolution grids. Int J Climatol 25:693–712

Ottoman Archives (1850–1930) Correspondences between Ottoman Palace and provinces (in Turkish). Directory of State Archives of Prime Ministry of Republic of Turkey

Purgstall BJVH (1983) Ottoman State History, Vol. 1–7, Translator: Vecdi Bürün, Üçdal Publishing, Istanbul (in Turkish)

Snee RD (1997) Validation of regression models: methods and examples. Technometrics 19:415–428

Stokes MA, Smiley M (1968) An introduction to tree-ring dating. University of Chicago Press, Chicago

Touchan R, Meko DM, Hughes MK (1999) A 396-year reconstruction of precipitation in Southern Jordan. J Am Water Resour Assoc 35:45–55

Touchan R, Garfin GM, Meko DM, Funkhouser G, Erkan N, Hughes MK, Wallin BS (2003) Preliminary reconstructions of spring precipitation in southwestern Turkey from tree-ring width. Int J Climatol 23:157–171

Touchan R, Funkhouser G, Hughes MK, Erkan N (2005a) Standardized precipitation indices reconstructed from Turkish tree-ring widths. Clim Change 72(3):339–353

Touchan R, Xoplaki E, Funkhouser G, Luterbacher J, Hughes MK, Erkan N, Akkemik Ü, Stephan J (2005b) Dendroclimatology and large-scale circulation influences in the eastern Mediterranean and Near East region. Clim Dyn 25:75–98

Touchan R, Akkemik Ü, Hughes MK, Erkan N (2007) May–June precipitation of South-Western Anatolia, Turkey during the last 900 years from tree rings. Quat Res 68(2):196–202

Touchan R, Anchukaitis KJ, Meko DM, Attalah S, Baisan C, Aloui A (2008) The long term context for recent drought in northwestern Africa. Geophys Res Lett 35:L13705. doi:10.1029/2008GL034264

Touchan R, Anchukaitis KJ, Shishov V, Sivrikaya F, Attieh J, Ketmen M, Stephan J, Mitsopoulos I, Christou A, Meko DM (2014) Spatial patterns of eastern mediterranean climate influence on tree growth. Holocene. doi:10.1177/0959683613518594

Weisberg R (1985) Applied linear regression. Wiley, New York

Wigley TML, Briffa KR, Jones PD (1984) On the average value of correlated time series, with applications in dendroclimatology and hydrometeorology. J Clim Appl Meteorol 23:201–213

Woodhouse CA, Gray ST, Meko DM (2006) Updated streamflow reconstructions for the upper Colorado River basin. Water Resour Res 42(5), Art. W05415

Xoplaki E, Gonzalez-Rouco JF, Luterbacher J, Wanner H (2004) Wet season Mediterranean precipitation variability: influence of large-scale dynamics and trends. Clim Dyn 23:63–78. doi:10.1007/s00382-004-0422-0